Geomechanics and Engineering, *Vol. 34, No. 2 (2023) 209-220*
https://doi.org/10.12989/gae.2023.34.2.209

Development of design chart for estimating penetration depth of dynamically installed Hall anchors in soft clays

Haijun Zhao[1], Zhaohan Zhu[2], Jiawei Che[*1], Wanchun Chen[1], Qian Yin[3], Dongli Guo[1], Haiyang Hu[1] and Shuang Dong[1]

[1]*China Construction Eight Engineering Division Rail Transit Construction Co., L.T.D., Nanjing, 210046, China*
[2]*School of Electrical Engineering, Southwest Jiaotong University, Chengdu, 611756, China*
[3]*Nanjing Metro, Nanjing, 210018, China*

(*Received February 3, 2023, Revised June 17, 2023, Accepted June 23, 2023*)

Abstract. In this study, a series of three-dimensional numerical analyses were carried out to investigate the penetration performance of a dynamically installed Hall anchor. The advanced coupled Eulerian-Lagrangian (CEL) technique was adopted to accurately simulate the large soil deformation during the vertical penetration of a Hall anchor. In total, 52 numerical analyses were conducted to investigate the relationship between anchor penetration depth and the initial kinematic energy. Moreover, a sensitivity analysis was performed to investigate the effects of soil shear strength and soil type on the penetration mechanism of a drop anchor under self-weight. There is a monotonic increase in the penetration depth with an increasing anchor weight when the topsoil of the riverbed is not subjected to erosion. On the other hand, all the computed depths significantly increase when soil erosion is taken into consideration. This is mainly due to an enhanced initial kinematic energy from an increased dropping depth. Both depths increase exponentially with the initial kinematic energy. An enhanced shear strength can potentially increase the side resistance and end-bearing pressure around a drop anchor, thus significantly reducing the downward penetration of a hall anchor. Design charts are developed to directly estimate penetration depth and associated plastic zone due to dynamically installed anchor at arbitrary soil shear strength and anchor kinematic energy.

Keywords: design chart; Hall anchor; kinematic energy; penetration mechanism; undrained shear strength

1. Introduction

Anchors have been frequently adopted to moor ships due to their low installation cost and high holding efficiency (Dou and Yu 2018). The penetration depth of an anchor is significant for the mooring of a large-scale ship. For example, submarine pipelines or cables may exist in the shallow depth of a riverbed, and excessive penetration of an anchor may collide with the existing utilities and pose significant threats to the serviceability of those facilities (e.g., Woo *et al.* 2009, Wang *et al.* 2021, Mustafina 2015, Moore *et al.* 2021). Therefore, it is imperative to have a sound understanding of anchor-soil interaction during the anchor installation process (Demir and Ok 2015, An *et al.* 2022).

Anchor installation can induce excessive disturbances to the riverbed and the penetration mechanism relies heavily on the anchor weight. The dynamical installation process mainly involves the free-fall penetration and follow-up drag penetration (Liu *et al.* 2010, Lai *et al.* 2021), and the embedment depth is intimately related to the kinematic behavior of anchors. Previous studies (Kim *et al.* 2015, Yue *et al*. 2020, Li *et al.* 2022) investigated the dynamic installation of torpedo anchors in cohesion soils. It was found that the anchor embedment depth was a function of the impact velocity, anchor geometric parameters and the undrained shear strength of riverbed sediments. The dynamic installation process could be decomposed into two separate stages. The first penetration stage (i.e., acceleration) was mainly driven by the self-weight of the anchor and mainly involved the mobilization of the end bearing mechanism, while the second stage (i.e., deceleration) was the formation of a cavity above the shaft and subsequent soil backflow. In addition, plate anchors (Lai *et al.* 2020), OMNI-max anchors (Liu *et al*. 2022), Hybrid plate anchors (Lai *et al*. 2021) have also been proposed to improve the holding capacity of large-scale offshore wind turbines. It was revealed that the Flying Wing plate anchors generally had deeper embedment depths than counterpart torpedo pile anchors and OMNI-max anchors. Clearly, the dynamical installation process of anchors is highly complex and a sound understanding of the penetration mechanism is crucial to the design of different anchors.

The prediction of anchor installation and its trajectory has been attracted extensive research attentions. The existing methods for the prediction could be essentially classified into three categories, namely empirical design charts (American Petroleum Institute 2005), analytical solutions based on plastic or equilibrium methods (Neubecker and Randolph 1995, Cassidy *et al*. 2012) and numerical simulations (Zhao and Liu 2016, Dou and Yu 2018). The former two approaches relied heavily on

*Corresponding author, Engineer
E-mail: chejiawei2023@163.com

ISSN: 2005-307X (Print), 2092-6219 (Online)

(a) Before anchor penetration (b) After anchor penetration

Fig. 1 Schematic diagram of vertical penetration of Hall anchor

engineering judgements or certain assumptions, which was hardly quantified rationally in practice. Numerical simulation was convenient and enabled detailed investigation of potential anchor-soil interaction at a minimal cost. However, the conventional finite element models in geotechnical engineering mainly were under the assumption of small-strain deformations. Thus, it was difficult to model the performance of geo-structures such as anchors.

Although extensive studies have been carried out to investigate the penetration mechanism of dynamically installed anchors, those studies mainly focused on experimental observations with empirical correlations. In this study, a series of numerical analyses were carried out to explore the penetration mechanism of dynamically installed anchors. The numerical model could accurately model large deformation and distortion of elements around a penetrating anchor, thus facilitating the quantification of influence depth and major plastic zones. A sensitivity study was carried out to investigate the effects of soil shear strength and soil type on the penetration mechanism. Based on the computed results, calculation charts were developed to estimate the penetration depth of hall anchor.

2. Landing velocity of Hall anchor

In this section, the typical anchoring process and the theoretical formulations for calculating the penetration depth are revisited. For a typical anchor installation process (Mohee *et al.* 2016), a ship anchor (e.g., Hall anchor) is connected by an installation line and released into the riverbed under the self-weight of an anchor. Upon the reach of the riverbed, the anchor continues to move but at a reduced rate due to the resistance from the water and riverbed. Subsequently, a vessel's forward motion causes tension in the line and forces the anchor to embed, thus exerting dragging force to the riverbed while accompanied by an increased embedment depth. In the ultimate state, the anchor does not penetrate any further, and the vessel stops.

Obviously, the anchor installation process is a complex and dynamic process. As a first approximation, a full anchor installation can be decomposed into several independent steps or a combination of vertical drop and horizontal drag. To simplify the complex dynamic problem, this study focuses on the vertical penetration process of a drop anchor under self-weight, as shown in Fig. 1. For a given soil stratum, the vertical penetration depth (h) is controlled by initial kinematic energy of the Hall anchor, which is determined by the landing velocity and weight of Hall anchor.

An anchor's ultimate penetration depth and associated anchor-soil interaction are highly reliant on the kinematic energy of a drop anchor. More specifically, the landing velocity is defined as the ultimate velocity of a drop anchor upon the reach of the riverbed. Note that once an anchor is released from a vessel, its vertical motion is mainly driven by gravity, and the water resistance or buoyance starts to work once the drop anchor falls into the water. Following the classical Newton's second law of motion, the landing velocity, v, of a drop anchor can be calculated as follows

$$v=\sqrt{2g\left[(h_1-\frac{U}{C_D A_f}\cdot\frac{(\rho_a-\rho_w)}{\rho_w})\cdot e^{-\frac{C_D A_f}{U(\rho_a+\rho_w)}h_2}+\frac{U}{C_D A_f}\cdot\frac{(\rho_a-\rho_w)}{\rho_w}\right]} \quad (1)$$

where g is the gravitational acceleration and takes on the value of 9.81 kg/m^2; ρ_a and ρ_w are densities of an anchor and the water, taking values of 7850 kg/m^3 and 1000 kg/m^3, respectively; U and A_f are the anchor volume and the projected horizontal cross-section of an anchor, both of which depend on the anchor type; C_d is a nondimensional resistance coefficient and quals 0.9; h_1 is the vertical distance between the anchor release point and the water surface; h_2 is the maximum water depth, depending on the specific design scenario (i.e., whether soil erosion exists or not).

3. Three-dimensional numerical analysis of anchor installation

All the numerical simulations were carried out using ABAQUS, which is an efficient numerical tool and has been frequently adopted to model soil-structure interactions (Kong *et al.* 2023a, Kong *et al.* 2023b, Kong *et al.* 2023c, Shi *et al.* 2022a). More importantly, ABAQUS has implemented the coupled Eulerian-Lagrangian (CEL) technique (Qiu *et al.* 2011, Dutta *et al.* 2015), which renders

Table 1 Summary of numerical analysis in this study

No.	Ship cargo capacity	Water condition	Anchor weight	Landing velocity	Kinematic energy
	10^4 ton		ton	m/s	kJ
Q3-1	3	No-erosion	6.0	6	108.0
Q3-2	3	Erosion	6.0	10.4	324.5
Q5-1	5	No-erosion	8.7	6.8	201.1
Q5-2	5	Erosion	8.7	10.6	488.8
Q10-1	10	No-erosion	14.7	7.5	413.4
Q10-2	10	Erosion	14.7	11.3	938.5
Q20-1	20	No-erosion	35.5	10.4	1919.8
Q20-2	20	Erosion	35.5	14.4	3680.6
Q40-1	40	No-erosion	33.0	9.7	1552.5
Q40-2	40	Erosion	33.0	13.8	3142.3

the explicit modelling of large deformations such as the anchor penetration in this study.

3.1 Program for numerical analysis

In this study, the main interest is the vertical penetration of a drop anchor under self-weight. Table 1 shows the test program in this numerical study. The ship's cargo capacity had a typical range of between 300,000 and 4,000,000 tons. Different water depths were adopted for the riverbed depending on whether the topsoil was subjected to soil erosion or not. The maximum water depth was calculated to be 29.18 m and 62.28 m for a non-erosional and erosional riverbed, respectively. The anchor weight was intimately linked to the ship's cargo capacity and ranged between 6 tons and 33 tons. Corresponding landing velocity was estimated following Eq. (1), which had a value of between 6 m/s and 14.4 m/s. All these values shown in Table 1 were representative of real conditions (Gao *et al.* 2019, An *et al.* 2022). It was convenient to represent the product of anchor weight and the square of landing velocity using a single term, i.e., kinematic energy.

3.2 Geology

The subsurface ground mainly consisted of soft silty clay, silty clay, and fine sand. For the riverbed free from erosion, the soft silty clay and the silty clay had thicknesses of 17.3 m and 19.0 m, respectively, underlain by a thick fine sand layer. On the other hand, if the surface soil layer, i.e., soft silty clay, was subjected to severe erosion, there would be a significant reduction in the total thickness from 17.3 m to 9.5 m. When the hall anchor was dynamically penetrated into clays, the clay with small permeability was under undrained conditions. Thus, the undrained shear strength was used for clays. In this study, a typical riverbed under Yangtse river was simulated (Gao *et al.* 2019, An *et al.* 2022). The sandy layer lay beneath the clay and silty clay layers. The effects of anchor penetration of sandy layer were negligible since the thickness of clay and silty clay layers were thick enough. Drained behavior was expected in sand with large permeability. Therefore, effective stress parameters were used for sand.

Table 2 Geotechnical properties of soil in this site

Soil Type	Constitutive model	Unit weight, γ (kN/m^3)	Young's modulus, E (MPa)	Effective frictional angle (^{0})	Undrained shear strength (kPa)
Soft silty clay	Mohr-Coulomb	17.3	3.7	/	12.0
Silty clay		18.3	5.2	/	18.0
Fine sand		19.5	10.2	34.9	/

Table 2 shows the soil parameters adopted in this study. Note that multiple samplings were extracted from the ground to determine the associated soil parameters, and the values in Table 2 were averaged from all the laboratory measurements. There were different kinds of vessel anchors available in the market. Among all the anchors, the Hall anchor gained wide popularity, particularly for large or mid-sized vessels due to its efficiency to hold the ground and its convenience for operation and storage. The weight of a Hall anchor was normally proportional to the cargo capacity of a vessel. For example, the minimal anchor weight for a 400,000-ton vessel was 33 tons (see Table 1).

The anchor in this study was assumed as an elastic material with a unit weight of 78.5 kN/m^3, Young's modulus of 207GPa, and a Poisson's ratio of 0.15.

3.3 Three-dimensional numerical mesh and boundary conditions

Fig. 2 shows the three-dimensional mesh of anchor-soil interaction. As shown in Fig. 2(a), the whole soil domain has a dimension of 100 m (length) × 100 m (width) × 100 m (height). All the soil layers and anchor were discretized using the EC3D8R element. Various mesh densities were applied to different zones, and the areas subject to the anchoring impact were densified (see Fig. 2(b)). In total, the three-dimensional mesh consisted of 922716 elements and 952200 nodes. When the number of the nodes and elements increased by 100%, the difference in the maximum penetration depth of the hall anchor was less than 2%. Thus, the mesh density chosen in the numerical analysis was already fine enough. The mesh density was considered adequate as any further refinement could only cause a minimal difference in the results. All four vertical side boundaries were restrained in the horizontal direction and were allowed to move freely in the vertical direction, while the bottom surface of the model was fixed in all directions. The top surface was free from any external constraints. Since hall penetration was a dynamic process, viscous boundaries were applied at the bottom and four vertical sides of the mesh, which is a typical boundary condition used for dynamic analysis (Cui *et al.* 2018, Cui *et al.* 2022, Cui *et al.* 2023, Meng *et al.* 2020).

The vertical free-falling anchor used in this study is shown in Fig. 2(c). The anchor was assumed as an elastic rigid body, whose deformation was considered negligible as compared with that of soils in contact. In total, each anchor consisted of 122752 elements and 181254 nodes. It was expected that the penetration depth of the hall anchor was greatly affected by the interaction behavior between the anchor and surrounding soils.

In this study, the normal behavior of the interface was

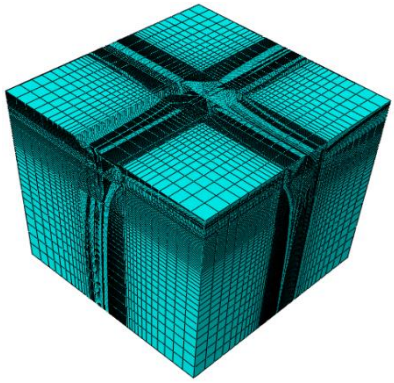

(a) Perspective view of the soil model

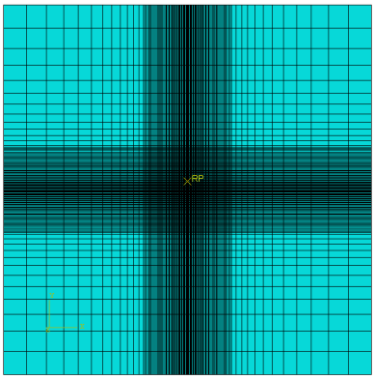

(b) Plan view of the soil model

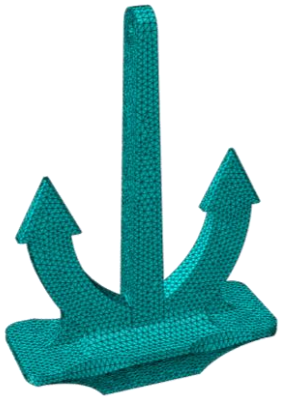

(c) Anchor

Fig. 2 Three-dimension numerical mesh of anchor-soil interaction

simulated by hard contact, while penalty formulation was used model the tangential behavior of the interface. Based on the previous studies, the interface frictional angle was taken as 2/3 of the soil frictional angle (Lu *et al.* 2019, Lu *et al.* 2020, Shi *et al.* 2022b, Shi *et al.* 2023, Zhou *et al*. 2023).

3.4 Numerical modelling procedures

To simplify the complex anchor-soil interaction and facilitate the convergence of the analysis, some key assumptions were made. For example, all the soil layers were taken homogeneous and isotropic, and the friction coefficient between an anchor and neighboring soils was constant. Before initiating the penetration, the anchor was assumed to hang up immediately over the riverbed level with an initial landing velocity as summarized in Table 1. The simulation proceeded until the penetration velocity reduced to zero. Some key simulation steps were summarized as follows:

(1) Build the anchor and soil model using the couple Eulerian-Lagrangian (CEL) technique and input pertinent material properties.

(2) Set up the initial boundary conditions and establish the initial geostatic earth stress conditions.

(3) Apply the initial landing velocity to the vertical loaded anchor and continue the penetration process until the kinematic energy of an anchor is fully dissipated.

(4) Carry out numerical analysis using parallel computing techniques.

4. Interpretation of computed results

Following the simulation procedures introduced in the foregoing subsection 3.4 and the test program in Table 1, 10 numerical analyses were carried out. Each analysis took about 24 hours using a laptop with 16 cores @ 3.5 GHz and 64G RAM.

4.1 Penetration mechanisms of a drop anchor under self-weight

Fig. 3 shows the temporal variation in the dissipation curve of kinematic energy for vessels with different cargo capacities. As shown in Figure 3a, the anchor for a 30,000-ton vessel exhibits a monotonic reducing trend in the kinematic energy regardless of soil erosion conditions. For case Q3-2, the initial kinematic energy is about 325 KJ, which is more than three times that of case Q3-1. This is because soil erosion occurred in case Q3-2, resulting in much larger falling depth of Hall anchor. As expected, large landing velocity is induced in the case of soil erosion. For both cases, the kinematic energy almost fully dissipates after about 0.35 second. The time required for a full dissipation of kinematic energy slightly increases to about 0.4 second when the ship cargo capacity increases to 50,000 tons. The same trends persist when the ship cargo capacity increases further to 400,000 tons, but the time required for a full dissipation of kinematic energy increases rapidly (i.e., about 1.0 s). This is because Hall anchor with large initial kinematic energy requires much longer time to penetrate to a deeper depth.

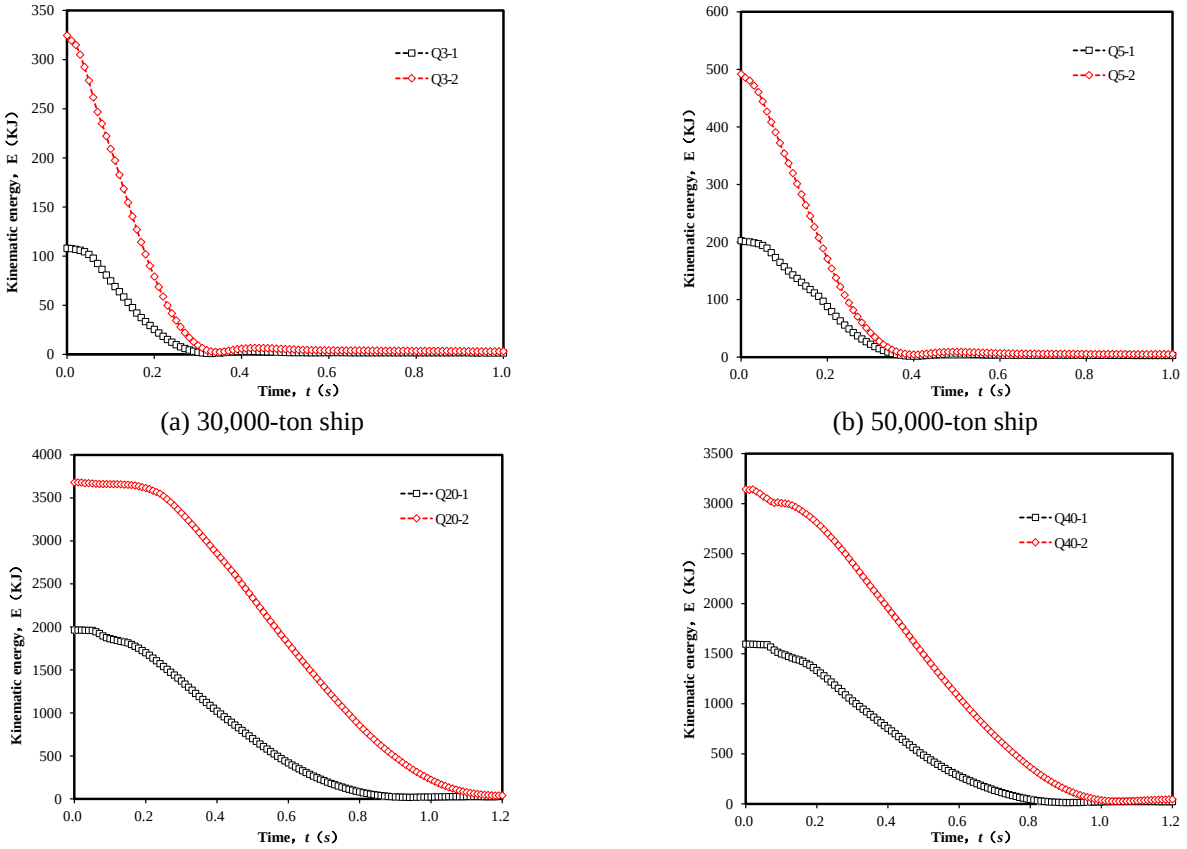

(a) 30,000-ton ship (b) 50,000-ton ship

(c) 200,000-ton ship (d) 400,000-ton ship

Fig. 3 Temporal variation in dissipation of kinematic energy

Fig. 4 shows the comparison of computed soil settlement and strain responses induced by a drop anchor for a ship with a cargo capacity of 30,000 ton (i.e., cases Q3-1 and Q3-2). As shown in Fig. 4(a), the overall penetration depth of the anchor is about 1.01 m. The stress bulb around the anchor in Fig. 4(b) indicates that the major plastic zone mainly concentrates with a small area around the anchor. The maximum depth of the plastic zone is around 2.28 m. In other words, the thickness of the plastic zone below the anchor is 1.27 m, which is of the same magnitude as the anchor penetration depth. It is also worthwhile to evaluate the total influence zone based on the contour of the von mises stress in Fig. 3(c). The depth of the influence zone surpasses the depth of the plastic zone in Fig. 3(b) by 1.84 m or 1.8 times the anchor penetration depth. Considering that the topsoil (i.e., soft silty clay) has a thickness of 17.3 m, the influence zone is relatively shallow and mainly concentrates within the soft silty clay layer.

In comparison, Figs. 4(d)-4(f) show the results for case Q3-2, of which the topsoil has a thickness of only 9.5 m due to soil erosion. The erosion causes a reduction in soil thickness and a concurrent increase in the water depth. Therefore, the initial kinematic energy of case Q3-2 significantly increases from 108 kJ to 324.5 kJ, and the penetration depth of a drop anchor also greatly rises from 1.01 m to 1.70 m. Similarly, the plastic zone slightly expands with the maximum plastic strain increased by 20% from about 0.91% to 1.10%. The stress bulb exhibits an elongation in the vertical direction. In addition, the max. von mises stress in Fig. 3(f) is about 3 times that in Fig. 3(c), corresponding influence depth slightly increases by 28.6% from 4.12 m to 5.30 m. For this given model geometry and soil stratum, the embedment depth of any submarine infrastructure should be larger than 5.3 m to prevent any potential damage caused by a drop anchor.

In practice, there are design codes used to estimate penetration depth of hall anchor. As the weight of hall anchor increases, the penetration depth increases as well. Table 3 gives the penetration depth of hall anchor with different weights in soft stratum (GB50217, 2018).

By using quadratic polynomial equation to fit the data shown in table 3, the relationship between the penetration depth of hall anchor and weight of hall anchor is described by Eq. (2).

$$Y = -0.0054X^2 + 0.3064X + 0.6389 \qquad (2)$$

where X is the weight of hall anchor, while Y is the penetration depth. In this study, the riverbed mainly consists of soft clay and silty clay. Using Equation (2), the penetration of hall anchor with different weights can be calculated.

Table 4 summarizes the influence depth induced by a drop anchor. In general, a heavy drop anchor has a relatively large kinematic energy, which tends to impose a large impact on the riverbed. For example, when the ship cargo capacity increases from 30,000 tons to 400,000 tons

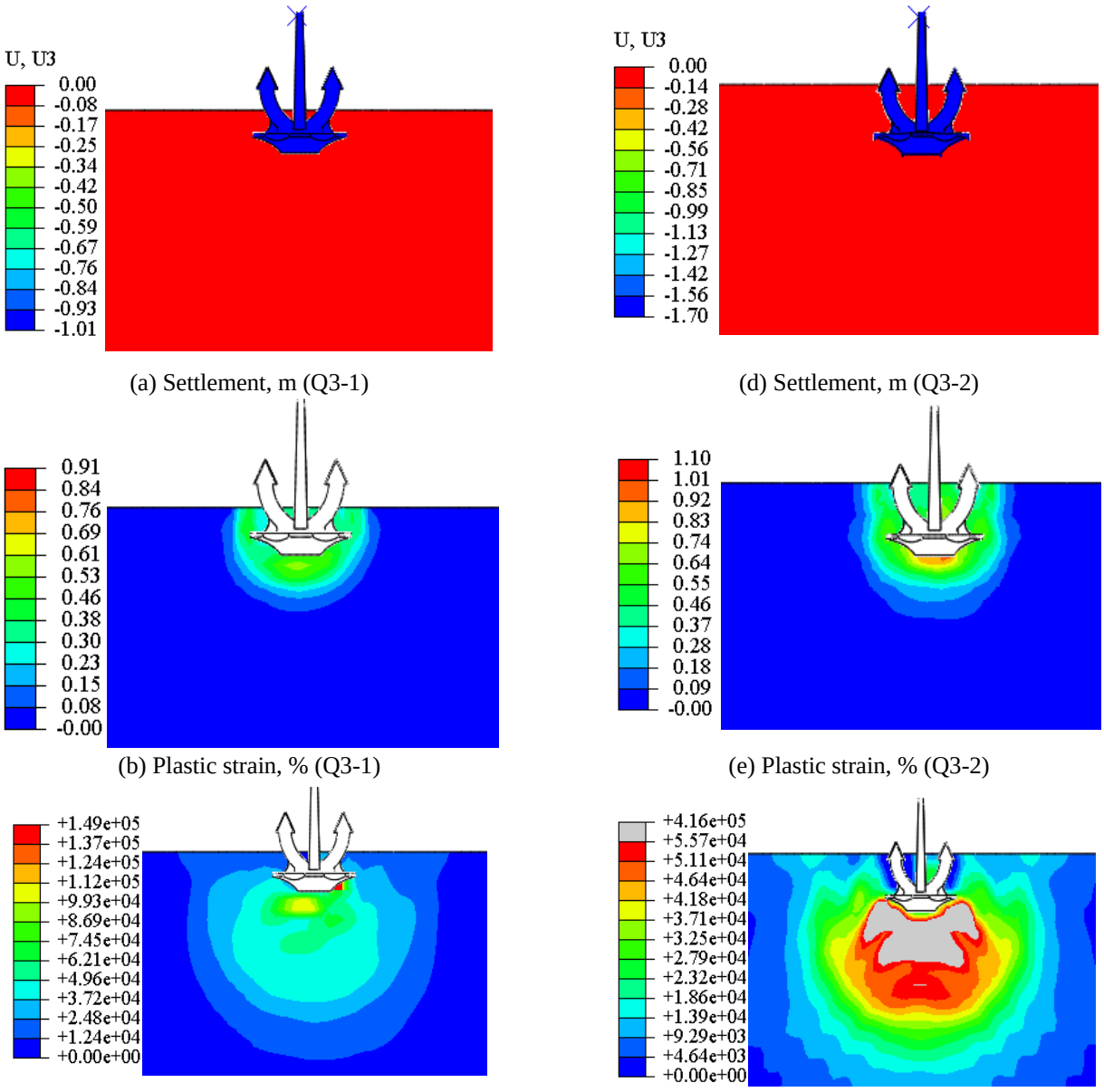

(a) Settlement, m (Q3-1) (d) Settlement, m (Q3-2)

(b) Plastic strain, % (Q3-1) (e) Plastic strain, % (Q3-2)

(c) Von mises stress, Pa (Q3-1) (f) Von mises stress, Pa (Q3-2)

Fig. 4 Comparison of computed penetration depth and plastic strain due to a drop anchor

in the absence of soil erosion, the kinematic energy monotonically increases from 108kJ to 1552.5kJ, and corresponding anchor penetration depth increases by 4 times from 1.01m to 4.09m. There is also a concurrent expansion in the depth of the plastic zone and influence depth. Although the kinematic energy rises by about 15 times, the depth of the plastic zone and the depth of influence zone only rise by 2.84 and 2.50 times. When soil erosion is taken into consideration, corresponding kinematic energy increases significantly, leading to a concurrent increase in the depth of the influence zone and anchor penetration depth. It is also worth mentioning that soil erosion does not necessarily result in an enhanced influence depth. For example, the influence depth of case Q40-2 is 9.5m, which is slightly smaller than that of case Q40-1. This can be explained by the fact that the silty clay layer immediately underneath the surface soft silty clay has better strength and stiffness, thus constraining the further propagation of the influence zone. It is noted that the existing guidelines significantly underestimate the penetration depth of a drop anchor as compared with the computed results in this study, which is mainly attributed to the fact that the landing velocity of a drop anchor has not been taken into consideration in the current engineering practice. Results from this study have significant practical implications. For example, submarine pipelines or cables may exist in the shallow depth of a riverbed, and excessive penetration of an anchor may collide with the existing utilities and pose significant threats to the serviceability of those facilities. The improved understanding of the anchor penetration mechanism in this study has helped develop practical design charts for anchor installation in coastal areas.

Table 3 Relationship between penetration depth and weight of hall anchor

Weight of hall anchor (ton)	0.2	0.5	1	15	30
Penetration depth of hall anchor (m)	0.5	0.75	1.2	4.0	5.0

Table 4 Summary of influence depth induced by a drop anchor

Case no.	Weight of hall anchor (Ton)	Kinematic energy (KJ)	Computed Penetration depth (m)	Penetration depth from design code (m)	Computed depth of plastic zone (m)	Computed influence depth (m)
Q3-1	6.0	108	1.01	2.28	2.28	4.12
Q3-2	6.0	324.5	1.70	2.28	3.25	5.30
Q5-1	8.7	201.1	1.43	2.90	2.83	5.18
Q5-2	8.7	488.8	2.03	2.90	3.75	6.45
Q10-1	14.7	413.4	1.92	3.98	3.68	6.45
Q10-2	14.7	938.5	2.93	3.98	4.94	7.91
Q20-1	35.5	1919.8	4.55	4.71	7.10	11.17
Q20-2	35.5	3680.6	6.79	4.71	9.00	9.70
Q40-1	33.0	1552.5	4.09	4.87	6.47	10.30
Q40-2	33.0	3142.3	6.01	4.87	8.57	9.50

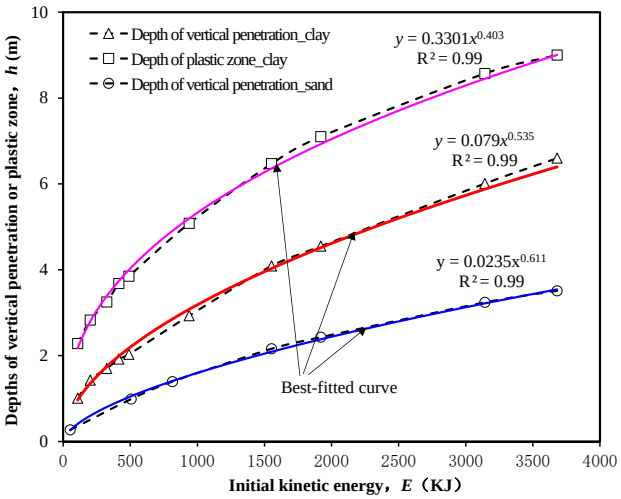

Fig. 5 Relationship between initial kinematic energy versus depths of vertical penetration and plastic zone

It is anticipated that the magnitude of anchor penetration depth is intimately linked to the initial kinematic energy. Fig. 5(a) shows relationship between initial kinematic energy and anchor penetration depth. The black dashed line with square markers denotes the computed anchor penetration depth, which exhibits an increasing trend with the initial kinematic energy but at a reducing rate. To facilitate engineering applications, an optimal curve in the form of an exponential line is obtained by fitting to the computed data with a correlation coefficient of more than 0.99, which indicates excellent fitting performance (i.e., the solid pink line, Eq. (3)). The obtained fitted curve has significant practical implications. In practice, in the absence of direct measurements or numerical simulation results, it is possible to directly utilize the fitted curve to back up the practical design if the anchor installation method and subsurface soil conditions are comparable.

Fig. 5(b) shows the relationship between initial kinematic energy and the depth of the soil plastic zone. As expected, the plastic zone develops rapidly when the kinematic energy increases from 0 to about 2000 kJ, after which the curve keeps rising but at a reduced rate. Similarly, the computed results can reasonably be fitted by an exponential curve (i.e., the solid pink line, Eq. (4)). Both the fitted curves shown in Fig. 5 provide useful guidance on determining influence depth for submarine infrastructures such as cables or subsea tunnels. Note that care should be exercised as the fitted curves are applicable only if similar soil conditions and anchor installation methods are adopted.

$$y = 0.3301x^{0.403} \tag{3}$$

$$y = 0.079x^{0.535} \tag{4}$$

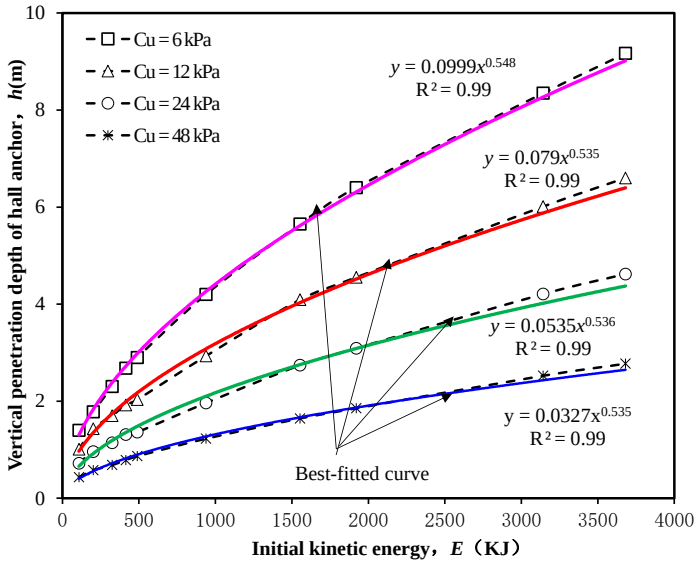

Fig. 6 Effects of undrained shear strength on penetration depth of a Hall anchor

Table 5 Summary of numerical parametric program

Weight of Hall anchor (ton)	Landing velocity (m/s)	Kinematic energy (KJ)	Undrained shear strength (kPa)
6.0, 8.7, 14.7, 33.0, 35.5	4.0~18.0	108~3680	6, 12, 24, 48

$$y = 0.0235x^{0.611} \quad (5)$$

It is worthwhile to compare the penetration mechanism of a drop anchor in different soil types. The dashed line with circles in Fig. 5 refers to the computed depth of vertical penetration in sand. There is a nonlinear increase in the penetration depth with the initial kinematic energy in sand. When the initial kinematic energy reaches about 3500 kJ, the corresponding penetration depth is about 3.2 m, which is only about a half of that in clay. This can be explained by the relatively high friction angle of sand. In other words, the anchor penetration in clay is more critical. In addition, the riverbed under Yangtse river typically consists of thick clay layers. Therefore, in this study, a series of sensitivity analyses were only carried out to investigate the effects of undrained shear strength of clays on the penetration mechanism of a drop anchor. It is also worth pointing out that only Hall anchors are considered in this study. The anchor geometry may also have a significant effect on the penetration mechanism of an anchor, which will be investigated in future studies.

5. Development of design chart for estimating penetration depth of Hall anchor

5.1 Three-dimensional numerical parametric program

The penetration mechanism of a drop anchor strongly depends on the shear strength of the topsoil of the riverbed. It is anticipated that the anchor penetration depth and associated plastic zone can be significantly altered if different riverbed materials are involved. Therefore, it is valuable to conduct a sensitivity study to investigate the variation in anchor penetration mechanisms subjected to different soil strengths. Table 5 summarizes all the parameters considered in this study. In this section, the silty clay's undrained shear strength (C_u) was allowed to change between 6 kPa and 48 kPa, i.e., half and double the original undrained shear strength (C_u = 12 kPa), respectively. To evaluate the effects of landing velocity on penetration depth, the landing velocity varies from 4.0 to 18.0 m/s. Note that natural riverbed soils typically have a low undrained shear strength, and the values adopted for sensitivity analysis represent the upper and lower bounds of soil strength for practical engineering design and analysis. In total, 40 three-dimensional numerical runs are conducted to develop the design chart.

5.2 Effect of velocity on vertical penetration of a Hall anchor

When erosion is occurred in the riverbed, the landing velocity increases rapidly, causing much large penetration depth. Thus, penetration depth of Hall anchor is controlled by a key parameter of landing velocity. Fig. 6 shows the relationship between depths of vertical penetration and plastic zone versus initial landing velocity. As an increase in the landing velocity, depths of vertical penetration and plastic zone increase almost linearly. Obviously, a large landing velocity causes much more initial kinematic energy.

5.3 Effect of undrained shear strength on vertical penetration of a Hall anchor

Fig. 6 shows the variation in the vertical penetration depth of a Hall anchor subjected to different undrained shear strengths (C_u). The dashed line with triangle markers is the benchmark and represents the computed result at C_u = 12 kPa.

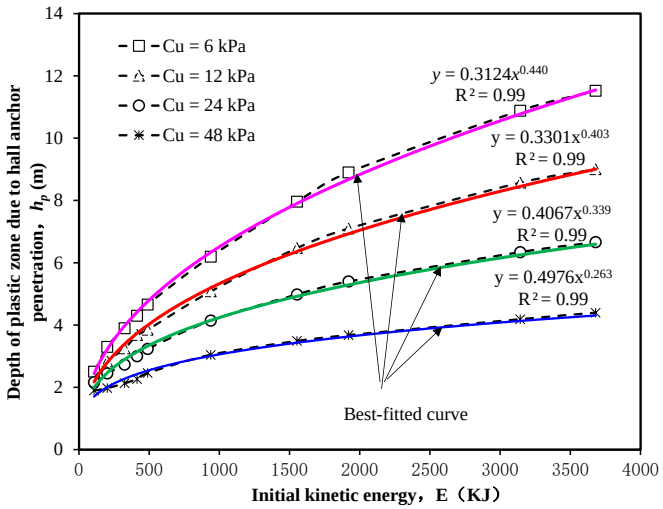

Fig. 7 Depth of induced plastic zone with initial kinematic energy

The vertical penetration depth of a Hall anchor is found to increase nonlinearly and monotonically with the initial kinematic energy. The nonlinear pattern is evident, particularly when the initial kinematic energy is less than 1000 kJ. When the undrained shear strength reduces to 6 kPa or half of the original shear strength, the vertical anchor penetration depth also has an increasing trend with rising initial kinematic energy, but the absolute magnitude is significantly larger than that with C_u = 12 kPa. For example, the vertical penetration depth significantly increases by 39.4% from 6.6 m to 9.2 m at a given initial kinematic energy of 3681 kJ when C_u reduces from 12 kPa to 6 kPa.

Similarly, the vertical penetration curve shifts downwards when the undrained shear strength doubles (C_u = 24 kPa and 48 kPa). However, the change in the penetration depth is not proportional to the variation in the undrained shear strength. More specifically, the vertical penetration depth decreases by up to 26% and 34%, respectively, when the undrained shear strength increases from 12 to 24 kPa and 24 to 48 kPa. Regardless of adopted undrained shear strengths, the computed penetration curves at different initial kinematic energy can reasonably be fitted by exponential functions with corresponding correlation coefficients of as high as 0.99, indicating excellent fitting performance. It implies that, in practice, a complete vertical penetration curve may be obtained by fitting an exponential curve to a limited number of measurements. In addition, the penetration curve for undrained shear strength other than the values as mentioned earlier (i.e., 6, 12, 24 and 48 kPa) may be directly interpolated from the three curves (Eqs. (6)-(9)) in Fig. 6.

$$y = 0.0999x^{0.548} \tag{6}$$

$$y = 0.079x^{0.535} \tag{7}$$

$$y = 0.0535x^{0.536} \tag{8}$$

$$y = 0.0327x^{0.535} \tag{9}$$

5.4 Effect of undrained shear strength on the depth of the plastic zone

The vertical penetration depth of a drop anchor has significant practical implications. The burial depth of any submarine structure, such as submarine cables, should be beyond the potential influence depth. Fig. 7 shows the variation in the depth of the plastic zone due to anchor penetration at different soil strengths. The dashed lines with triangle markers represent the development of plastic depth with the initial kinematic energy at C_u = 12 kPa. There is a monotonic increase in the computed depth of the plastic zone from about 2 m to 9 m when the initial kinematic energy, E, rises from 108 kJ to 3681 kJ. The depth is significantly larger than the anchor penetration depth in Fig. 6. For example, at E = 3681 kJ, the anchor penetration depth is 6.6 m or 73% of the total depth of the plastic zone.

Similarly, the depth of the plastic zone dramatically increases when the soil shear strength reduces by half, i.e., C_u = 6 kPa. The increase in the depth of the plastic zone is more evident as relatively larger initial kinematic energy. On the other hand, there is a concurrent downward shift in the depth of the plastic zone when the shear strength doubles from 12kPa to 48kPa. A strengthened ground can provide a larger side resistance and end-bearing force to dissipate the kinematic energy, thus resulting in a reduced anchor penetration depth (see Fig. 6) and plastic depth. The results in Fig. 7 indicate that the computed depth of the plastic zone at different initial kinematic energy can reasonably be fitted by exponential functions with high correlation coefficients irrespective of the soil shear strengths (Eqs. (11)-(13)). Note that all the results are computed using a Hall anchor but can be generalized to different types of anchors as long as the initial kinematic energy is comparable. In this study, the relationship between the kinematic energy and associated anchor penetration depth / plastic zone is established. The kinematic energy is directly related to the drop height and weight of an anchor. Based on the embedment depth of important infrastructures (e.g., submarine pipelines and

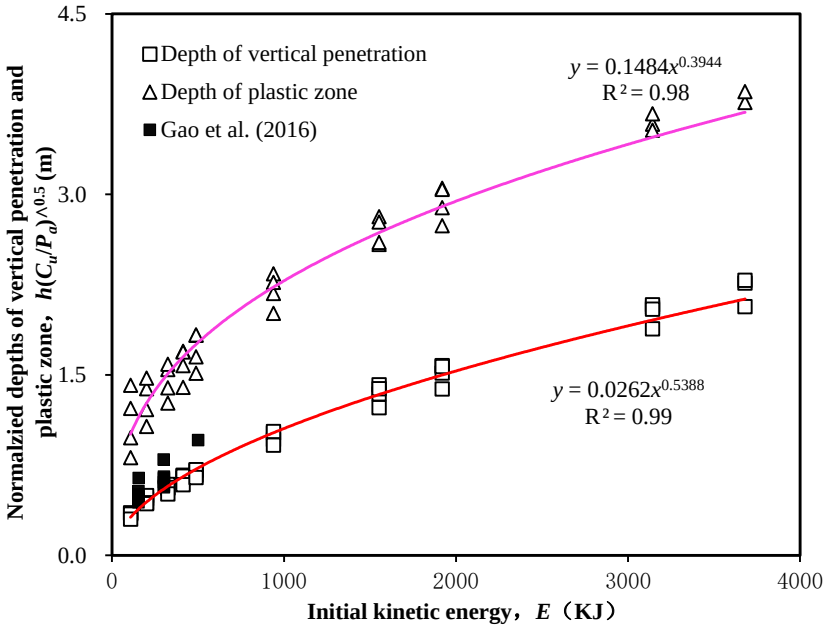

Fig. 8 Variation in the normalized depth with initial kinematic energy

cables) in the riverbed, the maximum allowable kinematic energy can be estimated, and engineers may inversely specify the anchor type and allowable maximum drop height. Note that this study is established based on ideal soil conditions without considering spatially varying soil properties and potential interbedded soil layer patterns (e.g., Shi and Wang 2021, 2022, 2023, Wang *et al*. 2023), which will be investigated in future studies.

$$y = 0.3124x^{0.440} \quad (10)$$

$$y = 0.3301x^{0.403} \quad (11)$$

$$y = 0.4067x^{0.339} \quad (12)$$

$$y = 0.4976x^{0.263} \quad (13)$$

5.5 Design chart for estimating penetration depth of Hall anchor

Note that the anchor penetration depth in Fig. 6 and the total depth of the associated plastic zone in Fig. 7 are heavily reliant on the soil shear strength. In practice, it may be worthwhile to unify all the computed depths at different strengths using a dimensional group or normalized depths.

It is found that all the results in above Figs. 6 and 7 can be concisely combined using a dimensional group, $h(C_u/P_a)^{0.5}$, where h is the anchor penetration depth or the depth of the plastic zone and P_a is a reference stress level (= 100 kPa). Fig. 8 shows the variation in the normalized depth with different initial kinematic energy. The square markers represent the normalized vertical penetration depth of a Hall anchor. All the computed points can reasonably be fitted by an exponential line, which is consistent with the findings in Figs. 6 and 7. There is a nonlinear increase in the normalized depth with the initial kinematic energy of a drop Hall anchor. Similarly, the depth of the plastic zone (i.e., triangle markers) can also be best fitted by an exponential curve (i.e., the pink line). In addition, Gao *et al*. (2016) carried out 3D numerical study to investigate the vertical penetration mechanism of Hall anchors in fine-grained materials, and the computed embedment depth has also been normalized and superimposed in Fig. 8 for comparison. It can be seen the results of Gao *et al.* (2016) mainly scatter around the best fitted line (i.e., the red solid line). In other words, the model parameters and modelling procedures adopted in this study are reasonable. It demonstrates that the dimensional group proposed in this study provides a unified indicator to concisely represent the performance of a drop Hall anchor and serves as a helpful vehicle to compare the performance of different anchors. Based on the limited numerical analyses, this calculation chart is developed to estimate the penetration depth of hall anchor. If soil parameters or hall geometry parameters are not within the ranges shown in Table 2, any extrapolation of the penetration depth of hall anchor should be treated with caution.

6. Conclusions

Anchor installation has been a key interest for offshore engineering, and a sound understanding of anchor-soil interaction during operation is crucial to the design and analysis of anchors as well as the planning of submarine infrastructures (e.g., telecables). In this study, a series of numerical analyses was carried out to investigate the mechanism governing an anchoring process. The large soil deformation during the anchoring process was modelled

using the coupled Eulerian-Lagrangian (CEL) technique. Based on the numerical results, the following conclusions may be drawn:

(1) There is a monotonic increase in the anchor penetration depth from 1.01 m to 4.09 m with an increase in the anchor weight from 6 tons to 33 tons when the topsoil of the riverbed is not subject to erosion. The depth of the plastic zone and total influence depth also exhibit a concurrent increase with an increase in the anchor weight. It is also found that all three depths (i.e., penetration depth, depth of plastic zone, and overall influence depth) significantly increase when the erosion in the topsoil is considered. This is mainly due to an enhanced initial kinematic energy from an increase in water depth.

(2) The vertical penetration depth of a Hall anchor and the associated depth of the plastic zone increase exponentially with the initial kinematic energy. Both depths are closely related to the shear strength of subsurface soils. An enhanced shear strength can potentially increase the side resistance and end-bearing pressure around a moving anchor, thus significantly reducing the downward penetration of a drop anchor.

(3) A dimensional group was proposed in this study to correlate the anchor penetration depth or depth of the plastic zone with initial kinematic energy. The newly proposed dimensional group can concisely combine all the penetration curves and serve as a useful vehicle for comparing the penetration mechanisms of different anchors. Designed charts are developed to directly estimate penetration depth and associated plastic zone due to dynamically installed anchor at arbitrary soil shear strength and anchor kinematic energy.

References

American Petroleum Institute. (2005), Design and analysis of station keeping systems for floating structures. API Recommended Practice 2SK.

An, X., Wang, F., Liang, C. and Liu, R. (2022), "Centrifuge modeling of dynamically penetrating anchors in sand and clay", *Geomech. Eng.*, **30**(6), 539-549. https://doi.org/10.12989/gae.2022.30.6.539.

Cassidy, M. J., Gaudin, C., Randolph, M. F., Wong, P. C., Wang, D. and Tian, Y. (2012), "A plasticity model to assess the keying of plate anchors", *Géotechnique*, **62**(9), 825-836. https://doi.org/10.1680/ geot.12.OG.009.

Cui, C.Y., Meng, K., Wu, Y.J., Chapman, D. and Liang, Z.M. (2018), "Dynamic response of pipe pile embedded in layered visco-elastic media with radial inhomogeneity under vertical excitation", *Geomech. Eng.*, **16**(6), 609-618. https://doi.org/10.12989/gae.2018.16.6.609.

Cui, C.Y., Liang, Z.M., Xu, C.S., Xin, Y. and Wang, B.L. (2023), "Analytical solution for horizontal vibration of end-bearing single pile in radially heterogeneous saturated soil", *Appl. Math. Model.*, **116**, 65-83. https://doi.org/10.1016/j.apm.2022.11.027.

Cui, C.Y., Meng, K., Xu, C.S., Wang, B.L. and Xin, Y. (2022), "Vertical vibration of a floating pile considering the incomplete bonding effect of the pile-soil interface", *Comput. Geotech.*, **150**, 104894. https://doi.org/10.1016/j.compgeo.2022.104894.

Demir, A. and Ok, B. (2015), "Uplift response of multi-plate helical anchors in cohesive soil", *Geomech. Eng.*, **8**(4), 615-630. https://doi.org/10.12989/gae.2015.8.4.615.

Dou, Y. and Yu, L. (2018), "Numerical investigations of the effects of different design angles on the motion behaviour of drag anchors", *Appl. Ocean Res.*, **76**, 199-210. https://doi.org/10.1016/ j.apor.2018.05.003.

Dutta, S., Hawlader, B. and Phillips, R. (2015), "Finite element modeling of partially embedded pipelines in clay seabed using Coupled Eulerian–Lagrangian method", *Can. Geotech. J.*, **52**(1), 58-72. https://doi.org/10.1139/cgj-2014-0045.

Gao, P., Duan, M.L., Gao, Q., Xu, J. and Huang, J. (2019), "A prediction method for anchor penetration depth in clays", *Ships Offshore Struct.*, **11**(7), 782-789. https://doi.org/10.1080/17445302.2015.1116244.

GB 50217. (2018), "Standard for design of cables of electric power engineering", Ministry of Housing and Urban-Rural Development of the People's Republic of China.

Han, C., Chen, X. and Liu, J. (2019), "Physical and numerical modeling of dynamic penetration of ship anchor in clay", *J. Waterway, Port, C-ASCE*, **145**(1):04018030. https://doi.org/10.1061/(ASCE)WW.1943-5460.0000490.

Kim, Y.H., Hossain, M.S., Wang, D. and Randolph, M.F. (2015), "Numerical investigation of dynamic installation of torpedo anchors in clay", *Ocean Eng.*, **108**, 820-832. https://doi.org/10.1016/j.oceaneng.2015.08.033.

Kong, G.Q., Fang, J.C., Lv, Z.X. and Yang, Q. (2023a), "Effects of pile and soil properties on thermally induced mechanical responses of energy piles", *Comput. Geotech.*, **154**, 105176. https://doi.org/10.1016/ j.compgeo. 2022.105176.

Kong, G.Q., Hu, S.J., and Yang Q. (2023b), "Uncertainty method and sensitivity analysis to assess building energy of underground metro station", *Sustain. Cities Soc.*, **92**, 104504. https://doi.org/10.1016/j.scs.2023. 104504.

Kong, G.Q., Wu, D. and Wei, Y.Q. (2023c), "Experimental and numerical investigations on the energy and structural performance of a full-scale energy utility tunnel", *Tunn. Undergr. Sp. Tech.*, **139**, 105208. https://doi.org/10.1016/j.tust.2023.105208.

Lai, Y., Huang, Y.H., Chen, C. and Zhu, B. (2020), "Free-fall penetration behaviors of a new dynamically installed plate anchor in marine clay", *China Ocean Eng.*, **34**(6), 795-805. https://doi.org/ 10.1007/s13344-020-0072-y.

Lai, Y., Zhu, B., Chen, C. and Huang, Y.H. (2021), "Dynamic installation behaviors of a new hybrid plate anchor in layered marine clay", *China Ocean Eng.*, **35**(5), 736-749. https://doi.org/ 10.1007/s13344-021-0065-5.

Li, G., Zhang, J., Niu, J., Liu, J. and Yang, Y. (2022), "Dynamic penetration process of torpedo anchors into sand foundation", *J. Mar. Sci. Eng.*, **10**(8), 1097. https://doi.org/10.3390/jmse10081097.

Liu, J., Liu, L. and Han, C. (2022), "Innovative booster for dynamic installation of OMNI-Max anchor in clay: numerical modeling", *J. Waterway, Port, C-ASCE*, **148**(1), 04021043. https://doi.org/10.1061/(ASCE)WW.1943-5460.0000691.

Liu, H., Zhang, W., Zhang, X. and Liu, C. (2010), "Experimental investigation on the penetration mechanism and kinematic behavior of drag anchors", *Appl. Ocean Res.*, **32**(4), 434-442. https://doi.org/ 10.1016/j.apor.2010.09.004.

Lu, H., Shi, J.W., Ng, C.W.W. and Lv, Y.R. (2020), "Three-dimensional centrifuge modeling of the influence of side-by-side twin tunneling on a piled raft", *Tunn. Undergr. Sp. Tech.*, 2020, **103**: 103486. https://doi.org/10.1016/j.tust.2020.103486.

Lu, H., Shi, J.W., Wang, Y. and Wang, R. (2019), "Centrifuge modeling of tunneling-induced ground surface settlement in sand", *Undergr. Space*, **4**, 302-309. https://doi.org/10.1016/j.undsp.2019.03.007.

Meng, K., Cui, C.Y., Liang, Z.M., Li, H.J. and Pei, H.F. (2020), "A new approach for longitudinal vibration of a large-diameter floating pipe pile in visco-elastic soil considering the three-

dimensional wave effects", *Comput. Geotech.*, **128**, 103840. https://doi-org/10.1016/j.compgeo.2020.103840.
Mohee, F.M., Al-Mayah, A. and Plumtree, A. (2016), "Anchors for CFRP plates: State-of-the-art review and future potential", *Compos. Part B: Eng.*, **90**, 432-442. https://doi.org/10.1016/j.compositesb. 2016.01.011.
Moore, E., Haigh, S.K. and Eichhorn, G.N. (2021), "Anchor penetration depth in sandy soils and its implications for cable burial", *Ocean Eng.*, **235**, 109411. https://doi.org/10.1016/j.oceaneng.2021.109411.
Mustafina, A. (2015). Anchor damage assessment of subsea pipelines-optimization of design methodology, Master's thesis, University of Stavanger, Norway.
Neubecker, S.R. and Randolph, M.F. (1995), "Profile and frictional capacity of embedded anchor chains", *J. Geotech. Eng.*, **121**(11), 797–803. https://doi.org/10.1061/(ASCE)0733-9410(1995)121:11(797).
Qiu, G., Henke, S. and Grabe, J. (2011), "Application of a Coupled Eulerian–Lagrangian approach on geomechanical problems involving large deformations", *Comput. Geotech.*, **38**(1), 30-39. https://doi.org/10.1016/j.compgeo.2010.09.002.
Shi, C. and Wang, Y. (2022). "Assessment of reclamation-induced consolidation settlement considering stratigraphic uncertainty and spatial variability of soil properties", *Can. Geotech. J.*, **59**(7), 1215-1230. https://doi.org/10.1139/cgj-2021-0349.
Shi, C. and Wang, Y. (2021), "Training image selection for development of subsurface geological cross-section", *Eng. Geol*., **295**(20), 106415. https://doi.org/10.1016/j.enggeo.2021.106415.
Shi, C. and Wang, Y. (2023), "Data-driven Spatio-temporal Analysis of Consolidation for Rapid Reclamation", *Géotechnique*, https://doi.org/10.1680/jgeot.22.00016.
Shi, J.W., Wang, J.P., Chen Y.H., Shi, C., Lu, H., Ma, S.K. and Fan, Y.B. (2023), "Physical modeling of the influence of tunnel active face instability on existing pipelines", *Tunn. Undergr. Sp. Tech.*, **140**, 105281. https://doi.org/10.1016/j.tust.2023.105281.
Shi, J.W., Wei, J.Q., Ng, C.W.W., Lu, H., Ma, S.K., Shi, C. and Li, P. (2022a), "Effects of construction sequence of double basement excavations on an existing floating pile", *Tunn. Undergr. Sp. Tech.*, **119**, 104230. https://doi.org/10.1016/j.tust.2021.104230.
Shi, J.W., Chen Y.H., Lu, H., Ma, S.K. and Ng, C.W.W. (2022b), "Centrifuge modeling of the influence of joint stiffness on pipeline response to underneath tunnel excavation", *Can. Geotech. J.*, **59**(9), 1568-1586. https://doi.org/10.1139/cgj-2020-0360.
Wang, W., Yan, X., Li, S., Zhang, L., Ouyang, J. and Ni, X. (2021), "Failure of submarine cables used in high-voltage power transmission: Characteristics, mechanisms, key issues and prospects", IET Generation, Transmission & Distribution, **15**(9), 1387-1402. https://doi.org/10.1049/gtd2.12117.
Wang, Y., Lyu, B., Shi, C. and Hu, Y. (2023), "Non-parametric simulation of random field samples from incomplete measurements using generative adversarial networks", *Georisk: Assessment and Management of Risk for Engineered Systems and Geohazards*, 1-25. https://doi.org/10.1080/17499518.2023.2222383.
Yue, L., Wang, Q., Wang, W., Wang, Y. and Lv, J. (2020), "Numerical simulation analysis of the characteristics of torpedo anchor penetration in cohesive Soil", *J. Coast. Res.*, **109**, 139-144. https://doi.org/ 10.2112/JCR-SI109-023.1.
Zhao, Y. and Liu, H. (2016), "Numerical implementation of the installation/mooring line and application to analyzing comprehensive anchor behaviors", *Appl. Ocean Res.*, **54**, 101-114. https://doi.org/10.1016/j.apor.2015.10.007.
Zhou, Y., Kong, G.Q. and Li, J.J. (2023), "Performances of belled pile influenced by pile head freedom response to a cooling-heating cycle", *J. Geotech. Geoenviron. Eng.*, **149**(2), 04022133. https://doi.org/ 10.1061/JGGEFK.GTENG-10407.

GC